Bifurcation structure of unstable periodic orbits in plane Couette flow with the Smagorinsky model

Eiichi Sasaki*
Graduate School of Engineering Science, Akita University, Akita 010-8502, Japan

Genta Kawahara
Graduate School of Engineering Science, Osaka University, Osaka 560-8531, Japan

Javier Jiménez
School of Aeronautics, Universidad Politécnica de Madrid, 28040 Madrid, Spain

(Received 17 July 2019; accepted 19 July 2021; published 25 August 2021)

To obtain insights into dynamics of developed plane Couette turbulence, this paper considers the bifurcation structure of unstable periodic orbits (UPOs) in the large-eddy-simulation (LES) system with the Smagorinsky-type eddy viscosity model. Treating the Smagorinsky constant as a bifurcation parameter, we detect the bifurcation points connecting two known UPOs which were separately discovered in the Navier-Stokes system [G. Kawahara and S. Kida, J. Fluid Mech. **449**, 291 (2001)]. At the moderately high Reynolds number, the LES UPO of the present study possesses the spanwise vortices, which seem to be caused by the streak instability and appear in the central region of the channel. We note that to our knowledge a spanwise vortex has not been reported through the UPO analysis of wall flows. The stretched spanwise vortices of the LES UPO enhance transfer of the streamwise turbulent momentum as in developed near-wall turbulence.

DOI: 10.1103/PhysRevFluids.6.084608

I. INTRODUCTION

Understanding developed Navier-Stokes (NS) turbulence is one of the key issues in the dynamical systems theory. The theory tells us that a countably infinite number of unstable periodic orbits (UPOs), to be exact invariant sets, are embedded in a chaotic attractor [1]. The stable and unstable manifolds of UPOs play roles of attractor and repeller for chaotic orbits, so the chaotic orbits wander around these UPOs like a pin ball in phase space. Therefore, UPOs represent dynamical properties of the chaotic attractor [2,3]. For the NS system, the solution orbits of a turbulent state pass through the neighborhood of UPOs, and the dynamical and structural properties of UPOs could describe representative motions and vortex structures of turbulence. Using the UPO analysis, we could obtain theoretical descriptions of the important events in developed turbulence. Here, we try to unveil essential dynamics of developed plane Couette turbulence through UPOs.

The approach based on the dynamical systems theory has succeeded especially in the characterization of low-Reynolds-number turbulence. The turbulent motions are sustained by creation and subsequent breakdown of the streaks; the so-called regeneration cycle [4,5]. In the early days of UPO analysis, a steady state was discovered [6–8], and this solution is sometimes called NCBW from the authors' names. We add that steady states are special cases of UPO without a period. The

*esasaki@gipc.akita-u.ac.jp

flow structure of NCBW consists of a wavy low-velocity streak and a pair of streamwise vortices, resembling the buffer-layer coherent structures in the near-wall region. Kawahara and Kida [9] examined plane Couette flow and found out two UPOs, one of which describes the regeneration cycle. Viswanath [10] presented other UPOs also explaining the regeneration cycle. In the past, a large number of UPOs reproducing the buffer-layer coherent structures have been reported and the review is given by Kawahara *et al.* [11]. For transition to turbulence in plane Couette flow of a large domain, turbulent spots and stripes are observed [12,13]. Their flow structures consist of spatially localized patches of unsteady complex flow within a background of laminar flow and they eventually decay. Brand and Gibson [14] reported an unstable steady state, which characterizes the localized coherent structure, and its stability depicts the transient growth and decay of turbulence. In addition, spatially localized solutions for wall-bounded shear flow have been found in pipe flow [15], channel flow [16], and square-duct flow [17]. Lustro *et al.* [18] identified the first appearance of a homoclinic tangency in plane Couette flow, which means the onset of transiently turbulent state that finally laminerizes. Using the rescaling of the Reynolds number, Eckhardt and Zammert [19] reported steady states and traveling waves, which localize in the wall-normal direction as the Reynolds number increases. Concerning turbulence control using dynamical systems theory Kawahara [20] demonstrated laminarization strategy for plane Couette flow. Recently, Linkmann *et al.* [21] applied this control protocol for channel flow. Note that we revisit work by Kawahara and Kida [9] later.

Our interest is in developed turbulence. When we use the conventional methods for the UPO analysis, we need "good" initial guesses which approximate the orbits of the target UPOs. In practice, the good initial guesses were obtained through heuristic methods. However, it is hard to identify turbulent orbits approaching UPOs at high Reynolds numbers. This study considers UPOs found at low Reynolds numbers, and we track their branches by increasing the Reynolds number.

The high degrees of freedom of developed turbulence are another difficulty for the UPO analysis. To decrease the degrees of freedom the present study employs the eddy viscosity model in the large-eddy simulation (LES). In the LES system, the large scales are computed on the resolved grid points, while the small-scale motions have to be modeled. The models describe the sub-grid-scale stress and the energy transfer between the grid scale and the sub-grid scale. One of the major models for sub-grid-scale stress is the Smagorinsky-type eddy viscosity [22]. This model has two parameters: the Smagorinsky constant C_S and the filter function with the filter width. In the case of homogeneous isotropic turbulence, Lilly [23] determined the Smagorinsky constant on the assumption that the grid scale lies within the inertial range of turbulence. For shear flow turbulence, however, an appropriate value of C_S may change from flow to flow [24,25]. In addition, the several types of the LES models have been studied [26–30]. We should note that checking the validity of these models, they carried out time integration of the NS and LES equations as prior and posterior tests. These tests have considered whether the LES turbulence gives good approximations for the NS turbulence with respect to their statistical properties such as the mean and root-mean-square (RMS) velocity profiles. Therefore, there is no guarantee that phase-space structure of the LES system could imitate that of the NS system.

The present study employs the static Smagorinsky-type eddy viscosity model [22], which is one of the canonical LES systems. We treat the Smagorinsky constant as a bifurcation parameter and study bifurcation structure of UPOs, although the static eddy viscosity is found to cause excessive damping of large-scale fluctuation. The statistical properties of LES turbulence are known to mimic those of NS turbulence, and the dynamics of LES flow resembles that of NS flow. If, in the LES system, we obtain UPOs embedded in the LES turbulent attractor, these dynamical properties could describe the LES turbulence, from which we could obtain some perspectives for the NS turbulence. Having similar motivations, Rawat *et al.* [31] presented as an LES steady state arising from NCBW, which represents the large-scale vortex structure in plane Couette flow. Hwang *et al.* [32] studied LES traveling waves in channel flow at very high Reynolds numbers, and they suggested that the large-scale structures could be explained using similar mechanisms of the buffer layer. For LES Taylor-Green flow in the three-dimensional (3D) torus, van Veen *et al.* [33] found a UPO describing

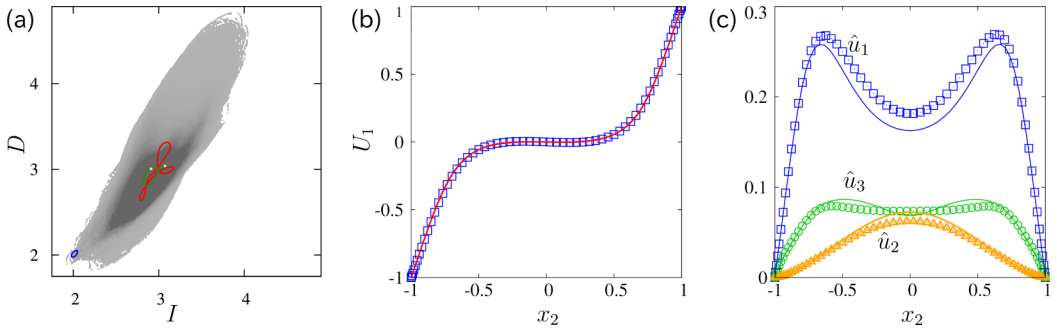

FIG. 1. Recalculation of Kawahara and Kida [9] and newly found UPOs using the number of grid points $(N_1, N_2, N_3) = (48, 65, 48)$. (a) Projection of the UPOs at $\mathrm{Re} = 400$. The horizontal and vertical axes represent the energy injection I and the energy dissipation D, respectively. The red and blue lines indicate the solution orbits of the vigorous and gentle UPOs [9], respectively. Furthermore, the green line means that of the active UPO, which is newly examined. All the orbits turn clockwise. The gray scale shows the probability density distribution of the NS turbulence. The two yellow dots on the green line shows the phases of panels in Fig. 6. (b) Mean velocity profile and (c) RMS velocity profiles at $\mathrm{Re} = 400$: the active UPO (lines), the NS turbulence (symbols).

pairs of antiparallel vortices, which represents the typical coherent structure on the turbulent energy transfer. Yang *et al.* [34] reported LES traveling waves in channel flow with a narrow spanwise computational domain. These traveling waves possess a self similarity with respect to the spanwise length at given Reynolds numbers.

This paper focuses on two UPOs reported by Kawahara and Kida [9] in the NS system. In the present study, we refer to these UPOs as the *vigorous* and *gentle* UPOs. The vigorous UPO is embedded in the turbulent attractor at the Reynolds number $\mathrm{Re} = 400$. Here, the Reynolds number is given by the half-distance of the channel height, the half-difference of the wall velocities, and the kinematic molecular viscosity. The statistical properties of the vigorous UPO approximate those of turbulence, and its dynamics explains the regeneration cycle. On the other hand, the gentle UPO is an edge state, which has only one unstable eigenmode. The edge state separates the turbulent and laminar states in the phase space. We should note that work by Viswanath [10] has questioned whether the vigorous UPO really exists at higher spatial resolutions. Figure 1 shows our recalculation results. We confirmed the existence of the vigorous UPO using the higher resolution than Kawahara and Kida's [9], but in Fig. 1(a) we could identify the slightly different shape of the projection orbit of the vigorous UPO from the original resolution. On the branch of the gentle UPO we detect a turning point at $\mathrm{Re} = 236.1$ where the gentle UPO connects to an upper branch through the saddle-node bifurcation. It now turns out that the gentle UPO is a lower branch of the saddle-node pair because it is closer to the laminar state than the upper one. Hereafter, we refer to the UPO on the upper branch of this pair as the *active* UPO, while only for the lower branch of this pair we use the gentle UPO. We stress that the active UPO is also embedded in the turbulent attractor at $\mathrm{Re} = 400$. The mean and RMS velocity profiles of this UPO approximate those of turbulence [Figs. 1(b) and 1(c)]. Therefore, we expect that not only the vigorous UPO but also the active UPO depict representative motions of turbulence at higher Reynolds numbers. The present study considers bifurcation structure of the vigorous, gentle and active UPOs in the LES system.

The remaining of this paper is organized as follows. The second section fixes the parameters and explains the numerical methods. In the third section we present the bifurcation structure of the UPOs. Treating the Smagorinsky constant as a bifurcation parameter, we discover that the vigorous UPO bifurcates from the active UPO in the LES system. At the moderately high Reynolds number, we track the branch of the LES active UPO with changing not only the Smagorinsky constant but also the number of grid points and so the filter width. The bifurcation structure seems similar for

different resolutions. These branches can be rescaled using the Smagorinsky mixing length. As the Smagorinsky constant decreases, the LES active UPO possesses the spanwise vortices created by the streak instability. The spanwise vortices are stretched by the streamwise vortices, leading to the high-Reynolds-stress objects attached to the walls. These results suggest that the spanwise vortices play a prominent role in the turbulent momentum transfer as in developed wall turbulence. The fourth section is devoted to conclusions.

II. SETUP

We consider the incompressible LES equation with the Smagorinsky model [24,35]

$$\frac{\partial u_i}{\partial t} + u_j \partial_j u_i = -\partial_i p + 2\partial_j \left\{ \left(\frac{1}{\mathrm{Re}} + \nu_e \right) S_{ij} \right\},$$
$$\partial_i u_i = 0,$$

where t is the time, $\vec{u} = (u_1, u_2, u_3)$ is the velocity, and p is the kinematic pressure. Here, $\partial_i = \partial/\partial x_i$ represents the spatial derivative with respect to x_i, where $\vec{x} = (x_1, x_2, x_3)$ indicates the streamwise, wall-normal, and spanwise coordinates, respectively, and $S_{ij} = (\partial_i u_j + \partial_j u_i)/2$ is the strain rate tensor. Quantities were normalized by the half-distance between the walls h and the half-difference of the wall velocities U, so that the Reynolds number is defined as $\mathrm{Re} = Uh/\nu$, where ν is the kinematic molecular viscosity. The dimensionless eddy viscosity ν_e is defined as

$$\nu_e = \{C_S \Delta(x_2) f_S(x_2)\}^2 |S|,$$

where $|S| = \sqrt{2S_{ij}S_{ij}}$. Moreover, C_S denotes the Smagorinsky constant, whose typical value seems to be in the range of 0.05 to 0.1 [24,25,31]. The filter width $\Delta(x_2) = \{\Delta_1 \Delta_2(x_2) \Delta_3\}^{1/3}$ is estimated in terms of the grid spacing, Δ_1, $\Delta_2(x_2)$, and Δ_3, in the streamwise, wall-normal, and spanwise directions. In addition, $f_S(x_2) = 1 - \exp(-x_2^+/A^+)$ is the van Driest damping function with $A^+ = 25$ [36]. The $^+$ superscript means quantities rescaled with the friction velocity u_τ and the kinematic molecular viscosity.

We impose periodic boundary conditions in the streamwise and spanwise directions and the nonslip and impermeability conditions at the walls: $u_i(x_1 + L_1, x_2, x_3) = u_i(x_1, x_2, x_3 + L_3) = u_i(x_1, x_2, x_3)$; $u_1(x_1, \pm 1, x_3) = \pm 1$; $u_2(x_1, \pm 1, x_3) = u_3(x_1, \pm 1, x_3) = 0$. We set the streamwise and spanwise periods to $L_1 = 1.755\pi$ and $L_3 = 1.2\pi$, which are a minimal flow unit at low Reynolds numbers [5,9].

The Chebyshev-Fourier-Galerkin spectral method is employed. We take the number of the grid points as $N_1 \geqslant 3K + 1, N_2 = L + 1, N_3 \geqslant 3M + 1$, and increase the resolutions up to $(N_1, N_2, N_3) = (50, 65, 50)$. Here, K, L, and M denote the streamwise, wall-normal, and spanwise truncation mode numbers, respectively. In addition, in our numerical setup, the implicit filtering is employed in the wall-normal direction, whereas in the wall-parallel directions the sharp cutoff filter is applied with the filter width equal to the grid size. Therefore, the wall-normal filter width $\Delta_2(x_2)$ is given by the grid spacing of the Gauss-Lobatto points, while the streamwise and spanwise ones are equally spacing $\Delta_1 = L_1/N_1$ and $\Delta_3 = L_3/N_3$. The time integration is carried out using the second-order Crank-Nicolson and Adams-Bashforth methods. To obtain UPOs, we use the Newton-GMRES method with the stopping condition expressed as

$$\frac{||\vec{\phi}_T(\vec{y}) - \vec{y}||}{||\vec{y}||} < 10^{-5}.$$

Here, $\vec{y} \in \mathbb{R}^D [D = 4(2K + 1)(L - 2)(2M + 1) + 2(L - 2)]$ is the state vector given by the real and imaginary parts of the spectral coefficients, $\vec{\phi}_T(\vec{y})$ is the time-T map defined by the time integration up to $t = T$ from the initial condition $\vec{y}$, and $||\vec{y}|| = (\vec{y}, \vec{y})^{1/2}$ is the Euclidean norm (see Ref. [37]). The GMRES method is a Krylov subspace method based on sparsity of simultaneous equations. As the number of grid points increases the dimension of Krylov subspace increases, implying that

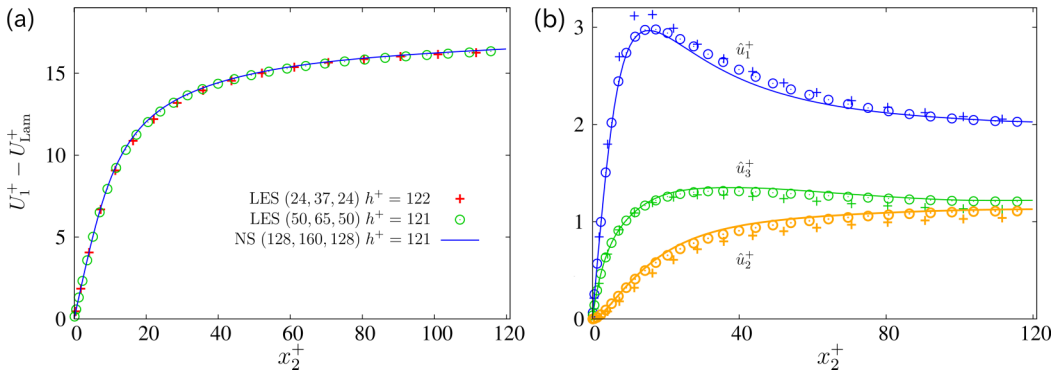

FIG. 2. Statistical properties of LES and NS turbulence at $\mathrm{Re} = 2000$ in our numerical computation. (a) Mean velocity profile. The linear laminar profile $U_{\rm Lam}^+$ has been subtracted. (b) RMS velocity profiles. The lines represent the NS turbulence for $h^+ = 121$, while the crosses and open circles denote the LES turbulence at $C_S = 0.1$ using the number of grid points $(N_1, N_2, N_3) = (24, 37, 24)$, $(h^+ = 122)$ and $(50, 65, 50)$, $(h^+ = 121)$, respectively. In panel (b), the blue, orange, and green colors indicate the RMS velocities $\hat{u}_1^+$, $\hat{u}_2^+$, and $\hat{u}_3^+$, respectively.

the UPO computation is numerically tough. For instance, to obtain a UPO at $\mathrm{Re} = 2000$ and $C_S = 0.2598$, we carry out 20 steps of the Newton iteration with the dimension of the Krylov subspace about up to 80 for each iteration. Here, we use the UPO at $\mathrm{Re} = 2000$ and $C_S = 0.2599$ as the initial guess. This calculation takes about three days using our computational resource.

Before presenting bifurcation structure of LES UPOs, we consider an optimal Smagorinsky constant in our numerical setup. Härtel and Kleiser [25] determined optimal Smagorinsky constants at different Reynolds numbers and spatial resolutions, taking into account equilibrium states on the overall exchange of the energy between the grid and sub-grid scales. Gullbrand and Chow [38] studied numerical error arising from different discretization methods, and they reported that the explicit filtering gives better approximation for the statistical properties. In this study, however, we only follow work by Deardorff [24] where he used $C_S = 0.1$. We carried out time integration of LES and NS equations for turbulent flows in the same domain size at several values of the Reynolds numbers. Figure 2 shows the mean and RMS velocity profiles of LES and NS turbulence at $\mathrm{Re} = 2000$. These profiles of the LES turbulence, which are obtained using $C_S = 0.1$ and the number of grid points $(N_1, N_2, N_3) = (24, 37, 24)$, resemble those of NS turbulence. In the case of $\mathrm{Re} \leqslant 1000$, $(N_1, N_2, N_3) = (24, 33, 24)$ is sufficient to achieve the good approximations for these profiles of the NS system.

III. BIFURCATION DIAGRAM OF LES UPOs

Let us start by examining LES UPOs with a fixed number of grid points, $(N_1, N_2, N_3) = (24, 33, 24)$ and so the filter width. We track the branches of the vigorous and gentle UPOs in the LES system and try to increase the Reynolds number. Figure 3 describes the bifurcation diagram, where the vertical axis indicates the maximal value of the cross-flow energy defined as

$$E_{\rm 2D}^{\rm max} = \max_{0 \leqslant t \leqslant T} \int \frac{u_2^2 + u_3^2}{2} \frac{\mathrm{d}V}{2L_1 L_3}.$$

The vigorous and gentle UPOs have two symmetries [9]

$$\Sigma_1 : (u_1, u_2, u_3)(x_1, x_2, x_3, t) \to (u_1, u_2, -u_3)(x_1 + L_1/2, x_2, -x_3, t),$$
$$\Sigma_2 : (u_1, u_2, u_3)(x_1, x_2, x_3, t) \to (-u_1, -u_2, u_3)(-x_1, -x_2, x_3 + L_3/2, t).$$

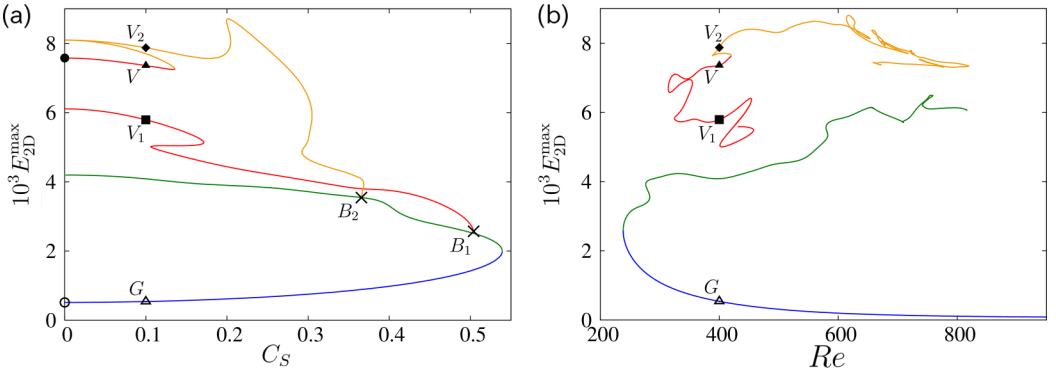

FIG. 3. Bifurcation diagram arising from the NS vigorous and gentle UPOs: (a) Re = 400, (b) $C_S = 0.1$. The solid and open circles represent the vigorous and gentle UPOs in the NS system ($C_S = 0$) [9], respectively. The blue and green lines represent the branches of the LES gentle and active UPOs arising through the saddle-node bifurcation. Additionally, the red line indicates the branch stemming from the NS vigorous UPO, while the orange line means the upper branch bifurcating from the branch of the LES vigorous UPO at the turning point. The solid triangles, solid squares, solid diamonds, and open triangles indicate the LES UPOs at Re = 400 and $C_S = 0.1$, which we call V, V_1, V_2, and G, respectively. The crosses on the branch of the LES active UPO in (a) represent the bifurcation points at $C_S = 0.5040$ and 0.3657, which we refer to as B_1 and B_2. To avoid needless confusion we omit numerous turning points and branches.

In addition, the gentle UPO possesses the following symmetry:

$$\Sigma_3 : (u_1, u_2, u_3)(x_1, x_2, x_3, t) \to (u_1, u_2, u_3)(x_1 + L_1/2, x_2, x_3, t + T/2).$$

At Re = 400 as the Smagorinsky constant increases from $C_S = 0$ [Fig. 3(a)], in the phase space of the LES system, the NS UPOs continuously connect to the LES UPOs. Here, we refer to the LES UPOs at $C_S = 0.1$ arising from the NS vigorous and gentle UPOs ($C_S = 0$) as V and G, respectively. Using the shooting method [39], we confirmed that the LES gentle UPO G is also an edge state as in the NS system. Tracking the branches originating from V and G, we detect two turning points at $C_S = 0.1358$ and 0.5393, where the corresponding upper branch arises from each branch. We refer to the solution of the upper branch of the saddle-node pair arising from G as the LES active UPO, while the lower one is the LES gentle UPO. Note that the branch of the LES active UPO connects to the NS active UPO at $C_S = 0$. On the branch of the LES active UPO, we detect two bifurcation points at $C_S = 0.5040$ and 0.3657, which we call B_1 and B_2, respectively. At each bifurcation point, a UPO bifurcates with breaking the symmetry Σ_3. Tracking the branch bifurcating from B_1, we find an LES UPO at $C_S = 0.1$, which we refer to as V_1. Next, changing the Reynolds number with fixing $C_S = 0.1$ [Fig. 3(b)], we figure out that the branch stemming from V_1 connects with V. Moreover, on the branch originating from B_2 we also identify an LES UPO V_2 at $C_S = 0.1$ and the connection from V_2 to V by varying the Reynolds number. We determine that in the phase space of the LES system, the gentle UPO connects to the vigorous UPO through the branches stemming from B_1 and B_2. Note that Kawahara and Kida [9] separately examined the vigorous and gentle UPOs in the NS system, and therefore, the relevance between them was unknown. This result suggests that introducing the eddy viscosity model has led to nontrivial solutions and their relationship, and that the eddy viscosity could be a useful homotopy parameter for searching novel UPOs to the NS equations.

In Fig. 3(b), as the Reynolds number increases we identify the appearance of complicated behavior of the upper branches and resulting several turning points especially at $600 \leqslant \mathrm{Re} \leqslant 800$. This implies an insufficient resolution. In addition, we confirmed that the magnitude of the eddy viscosity is less than approximately 10% of that of the kinematic molecular viscosity. This indicates that the eddy viscosity does not work well. The assumption of the LES models is that the grid scale

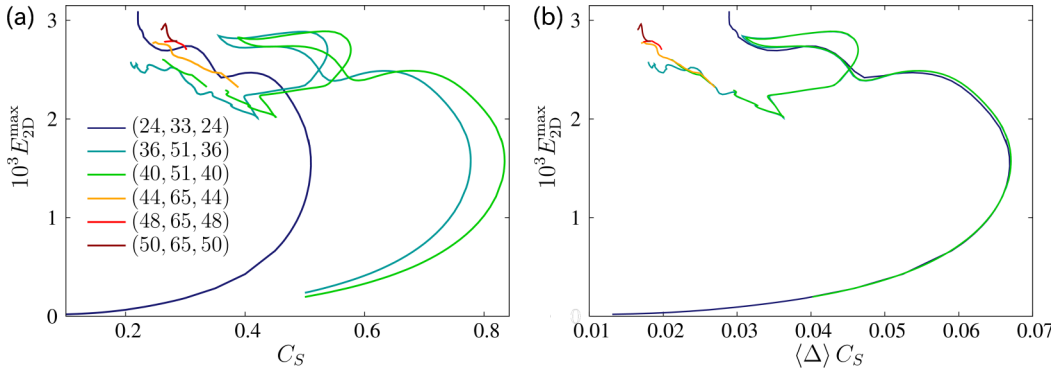

FIG. 4. Bifurcation diagram of the LES gentle and active UPOs at Re = 2000. The colored lines, from dark-blue to dark-red, represent the sets of the number of grid points from $(N_1, N_2, N_3) = (24, 33, 24)$ to (50,65,50), and so the filter widths.

lies within the inertial range of turbulence. At low Reynolds numbers, however, the sub-grid scale is comparable to the viscous scale, and therefore, the assumption is not valid. In this sense, the failure of the eddy viscosity model is reasonable. Then, we stopped tracking the upper branches, but pursue the branch of the LES gentle UPO up to Re = 2000. We note that it is easy to track the lower branch without the eddy viscosity because the lower-branch solution does not have small-scale structures. As shown in the introduction, the active UPO, the upper branch arising from the gentle UPO, approximates the mean and RMS velocity profiles of NS turbulence at Re = 400. We expect that the active UPO could also depict turbulent motions at high Reynolds numbers. Using the Smagorinsky constant as the bifurcation parameter, we investigate the branch of the LES gentle UPO at Re = 2000 and find out the LES active UPO arising from the LES gentle UPO through the saddle-node bifurcation.

We track the branches of the LES gentle and active UPOs changing the number of grid points and so the filter width. Figure 4 shows the bifurcation structure at Re = 2000. Using the shooting method we confirm that the LES gentle UPO at Re = 2000 and $C_S = 0.1$ is an edge state as in the NS system at Re = 2000. Changing the Smagorinsky constant we find that the LES active UPO arises as the saddle-node bifurcation pair with the LES gentle UPO at a finite Smagorinsky constant. Moreover, the branches exhibit similar behaviors for various resolution [Fig. 4(a)]. We discover that these branches can be rescaled using the Smagorinsky mixing length $\langle\Delta\rangle C_S$. Here, $\langle\Delta\rangle$ indicates the averaged filter width

$$\langle\Delta\rangle = \left(\frac{2L_1L_3}{N_1(N_2-1)N_3}\right)^{1/3}.$$

If we use the sufficient number of grid points, the bifurcation structure is robust against the resolution and the eddy viscosity does not violate the phase space structure of the LES system. To check the validity of sub-grid-scale models, the statistical properties of LES turbulence were examined. Using the UPO analysis we could assess proper resolution with respect to the phase space structure in the LES system. Note that the saddle-node bifurcation point of the pair of the LES gentle and active UPOs is at $\langle\Delta\rangle C_S \simeq 0.067$. We study the LES active UPO by decreasing the Smagorinsky constant.

The LES active UPO is embedded in the LES turbulent state at Re = 2000. Figure 5 shows representative snapshots of the LES active UPO at Re = 2000, $\langle\Delta\rangle C_S = 0.05$ ($C_S = 0.5797$, $(N_1, N_2, N_3) = (36, 51, 36)$). The spatial structure exhibits the a pair of positive and negative streamwise vortices and the meandering streak. Figure 6 displays the snapshots of the NS active UPO at Re = 400 for comparison purposes. The flow structure of the LES active UPO resembles

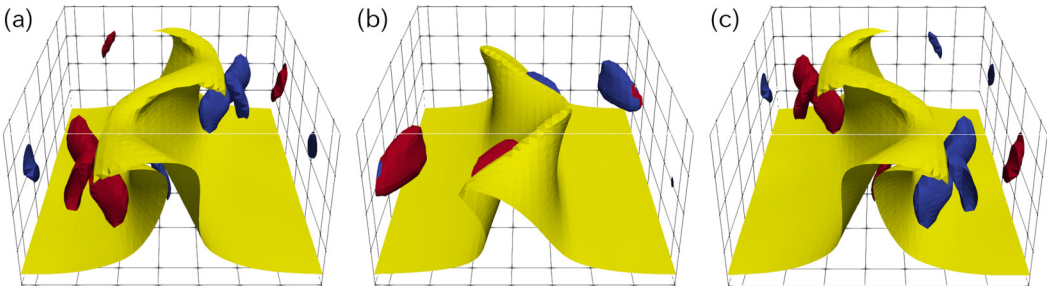

FIG. 5. Snapshots of the LES active UPO of the period $T = 93.72$ at $\mathrm{Re} = 2000$ and $\langle\Delta\rangle C_S = 0.05$ ($C_S = 0.5797$, $(N_1, N_2, N_3) = (36, 51, 36)$, $h^+ = 136$): (a) $t = 0$, (b) $t = T/4$, and (c) $t = T/2$. The yellow object denotes the isosurface of the streamwise velocity $u_1 = 0.15$ ($u^+ = 12.5$), while the red and blue objects represent the vortical structure visualized by the isosurfaces of the second invariant of velocity gradient tensor $Q = 0.05$ with the positive and negative streamwise vorticity.

the NS one, although the dissipation mechanism of the LES system is different from that of the NS system. We add that the energy injection and the cross-flow energy of the LES active UPO are about twice larger than those of the NS UPO. This result implies that the eddy viscosity in the overdamped LES system quenches the small-scale vortices, so the flow structures of them seem similar.

As the Smagorinsky constant decreases using the low resolutions, we identify the appearance of complicated behavior on the upper branch, again. Therefore, we try to decrease the Smagorinsky mixing length and increase the number of the grid points till the practical numerical cost. We track the branch down to $\langle\Delta\rangle C_S = 0.01658$ [$C_S = 0.2598$, $(N_1, N_2, N_3) = (50, 65, 50)$]. Figure 7 presents the projection of the solution orbit of the LES active UPO on the plane spanned by the energy injection I and the cross-flow energy $E_{2\mathrm{D}}$, where $I = \int\int(\partial u_1/\partial x_2|_{x_2=1} + \partial u_1/\partial x_2|_{x_2=-1})\mathrm{d}x_1\mathrm{d}x_3/2L_1L_3$. The solution orbit of the LES active UPO seems to be embedded in the LES turbulent attractor. Moreover, Fig. 8 plots the mean and RMS velocity profiles. We could find that the mean and RMS velocity profiles of the LES active UPO nicely fit those of the LES turbulence. However, these profiles of the LES turbulence do not approximate those of the NS turbulence because of the slightly large Smagorinsky constant (see also Fig. 2). We expect that the LES active UPO provides some insights into the dynamics of NS turbulence despite these discrepancies.

Figure 9 shows the typical snapshots of the LES active UPO. We could find more prominent streak motions and vortical structures than in Fig. 5. From Figs. 9(a) to 9(d), the streak, the yellow objects, becomes wavy driven by the streamwise vortices, and from Figs. 9(e) to 9(g),

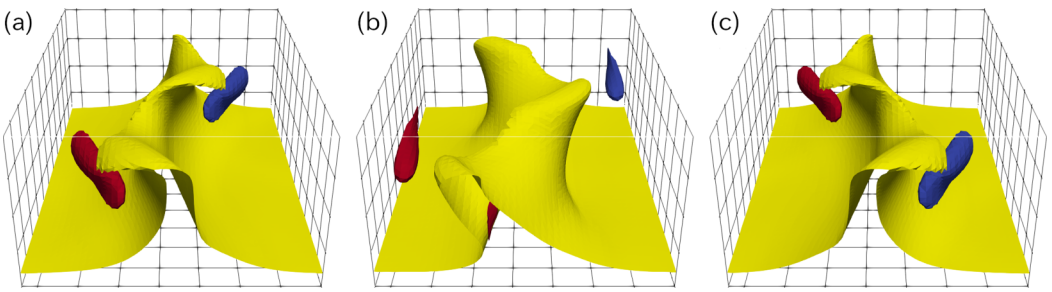

FIG. 6. Snapshots of the NS active UPO of the period $T = 62.13$ at $\mathrm{Re} = 400$ ($h^+ = 35.0$): (a) $t = 0$, (b) $t = T/5$, and (c) $t = T/2$. The definition of isosurfaces is the same as Fig. 5, but $u_1 = 0.2$ and $Q = 0.2$. See also Fig. 1.

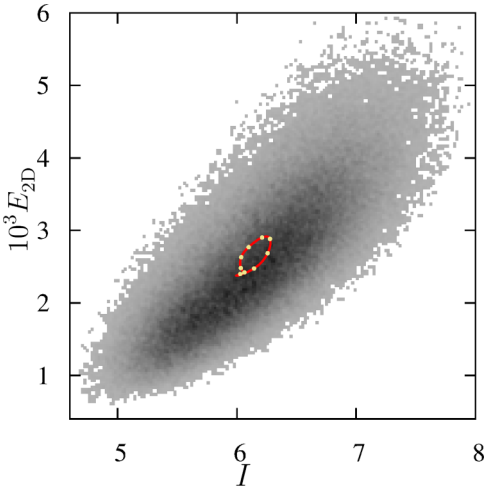

FIG. 7. Projection of the LES active UPO at $\mathrm{Re} = 2000$ and $\langle\Delta\rangle C_S = 0.01658$ ($C_S = 0.2598$, $(N_1, N_2, N_3) = (50, 65, 50)$, $h^+ = 105$). The horizontal and vertical axes mean the energy injection I and the cross-flow energy E_{2D}. The red line indicates the solution orbit of the LES active UPO. The gray scale shows the probability density distribution of the LES turbulence for $h^+ = 110$. The yellow dots represent the phases of panels (a) to (i) in Fig. 9. The orbit turns counterclockwise.

we can identify the spanwise vortices in the central region of the channel. The wavy streak and spanwise vortices seem to be caused by the streak instability [41]. Figure 10 represents the detail of development of the spanwise vortices. The pair of the streamwise vortices stretches and intensifies the spanwise vortices. We should stress that to our knowledge a spanwise vortex has not been reported through the UPO analysis of wall flows. From Figs. 9(h) to 9(i), it can be seen that the spanwise vortices reach the vicinity of the other walls and eventually decay.

The streak dynamics represents the streamwise-momentum transfer through turbulent fluctuation. To figure out the relation of the turbulent momentum transfer and the spanwise vortical

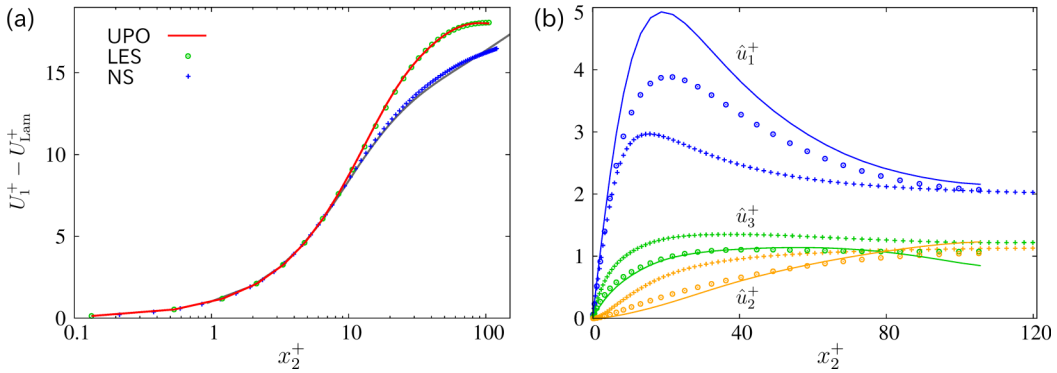

FIG. 8. (a) Mean velocity and (b) RMS velocity at $\mathrm{Re} = 2000$. The lines mean the LES active UPO at $\mathrm{Re} = 2000$ and $\langle\Delta\rangle C_S = 0.01658[C_S = 0.2598,\ (N_1, N_2, N_3) = (50, 65, 50),\ h^+ = 105]$, while the open circles represent the LES turbulence ($h^+ = 110$) at the same parameters. Additionally, the crosses signify the NS turbulence in our numerical computation, already shown in Fig. 2. In panel (a), the gray line indicates the NS turbulence for $h^+ = 550$ of the large domain [40], whereas in panel (b), the definition of colors is the same as Fig. 2(b).

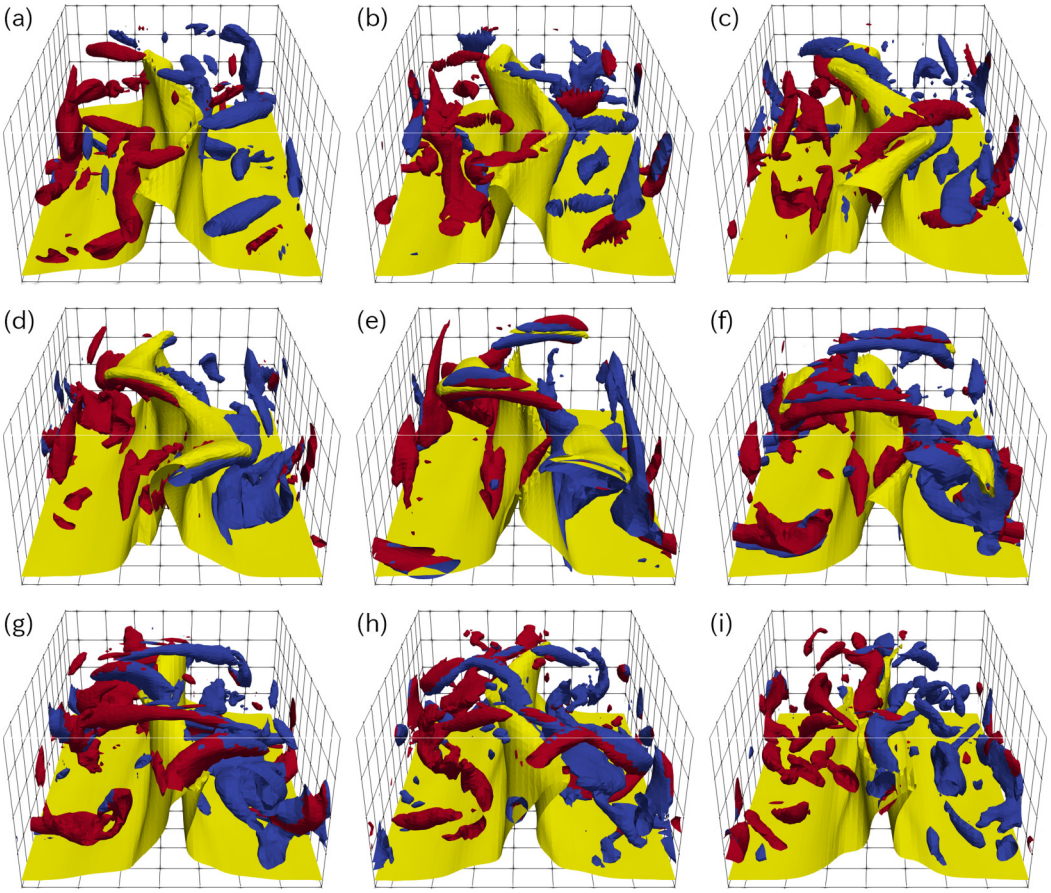

FIG. 9. Snapshots of the LES active UPO of the period $T = 79.25$ at $\mathrm{Re} = 2000$ and $\langle\Delta\rangle C_S = 0.01658$ [$C_S = 0.2598$, $(N_1, N_2, N_3) = (50, 65, 50)$, $h^+ = 105$]. Time elapses from (a) to (i) by $T/20$. The definition of isosurfaces is the same as Fig. 5, but $u_1 = 0.2$ ($u^+ = 21.6$) and $Q = 0.1$.

structure, we consider the momentum transport by turbulent fluctuations. In the averaged equation of the streamwise velocity, the derivative of the Reynolds shear stress $-u_1'u_2'$ is the source term for the turbulent fluctuation. Here, u_i' is the fluctuation velocity. Hence the large Reynolds stress means the prominent modulation of the turbulence from the mean flow. Figure 11 shows the isosurfaces of the rescaled Reynolds shear stress [42]

$$\frac{|u_1'(\vec{x})u_2'(\vec{x})|}{\hat{u}_1(x_2)\hat{u}_2(x_2)} = 1.75,$$

where $\hat{u}_i$ signifies the RMS velocity. The high-Reynolds-stress objects are embedded in the streaks and sandwiched between the streamwise vortices. When the spanwise vortices are created in the central region of the channel, the high-Reynolds-stress objects attach to the walls. These results imply that the appearance of the spanwise vortices is the trigger of the significant momentum transfer. In fully developed turbulence, the spanwise vortices were observed mainly in the overlap region apart from the wall [43]. We expect that the spanwise vortices of the LES active UPO could represent the key events of developed turbulence, although it is not clear whether the dynamics of the present UPO is strictly consistent with that in near-wall turbulence at higher Reynolds numbers.

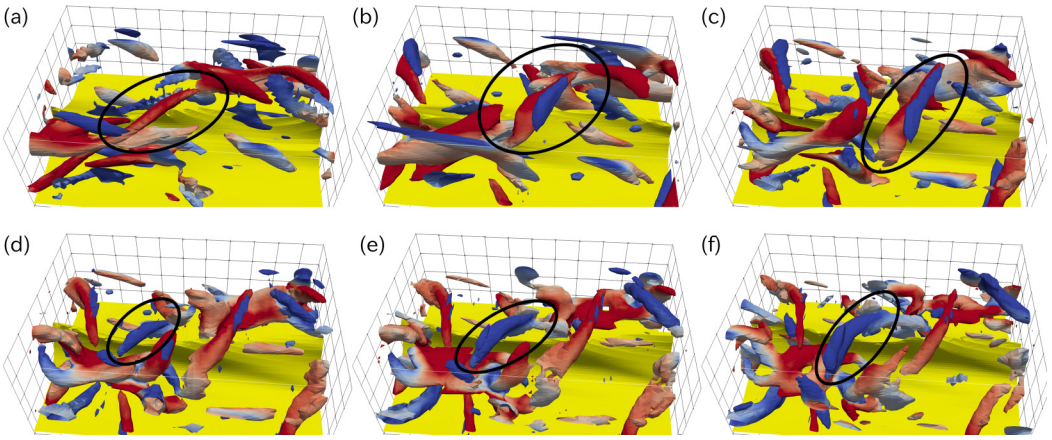

FIG. 10. Development of spanwise vortices. The yellow objects are the isosurfaces of the streamwise velocity $u_1 = 0.3$, while the blue to red objects denote $Q = 0.1$ within the range of $-0.75 \leqslant \omega_3 \leqslant 0.75$. Time elapses from (a) to (c) by $T/20$ ($3T/20 \leqslant t \leqslant 5T/20$) and from (d) to (f) by $T/40$ ($55T/200 \leqslant t \leqslant 65T/200$). The black circles are used for emphasis on the spanwise vortices.

IV. CONCLUSION

Toward perspectives of dynamical properties of turbulence, we herein document the bifurcation structure of unstable periodic orbits (UPOs). To decrease the degrees of freedom we consider the large-eddy simulation (LES) with the Smagorinsky-type eddy viscosity model. Treating the Smagorinsky constant as a bifurcation parameter, we study bifurcation structure of UPOs at moderately high Reynolds number.

We demonstrate that the vigorous UPO bifurcates from the branch of the newly examined active UPO arising from the gentle UPO as the saddle-node pair in the LES system. We note that the vigorous and gentle UPOs were separately unveiled by extraction from the chaotic attractor [9]. This result suggests that the eddy viscosity model could present a useful homotopy parameter for searching UPOs, and we could seek novel nonlinear solutions and their relationship.

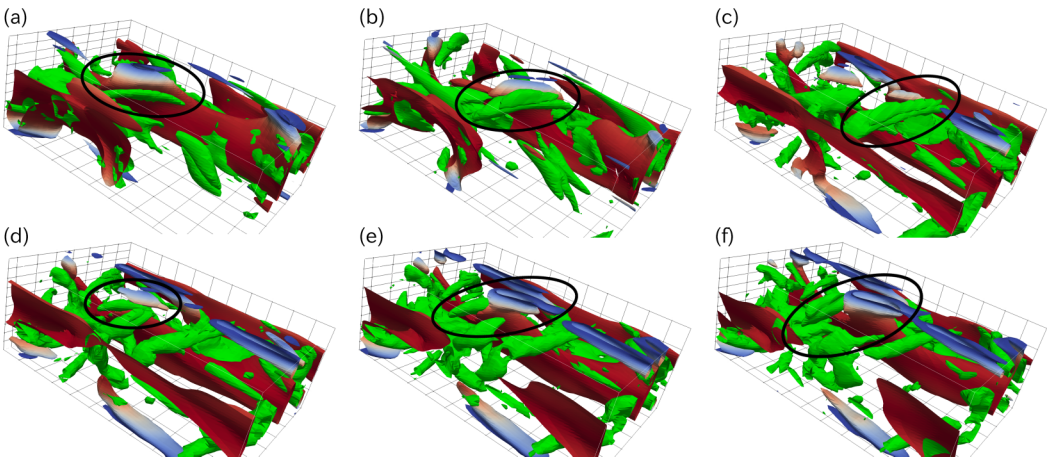

FIG. 11. Reynolds shear stress $-u_1'u_2'$ of the LES active UPO. The blue to red objects indicate the isosurface $|u_1'u_2'|/(\hat{u}_1\hat{u}_2) = 1.75$ where the color means the value of the Reynolds shear stress $-u_1'u_2'$ from 0 to 0.014. The green surfaces indicate $Q = 0.1$. The time series of (a) to (c) and of (d) to (f) are the same as Fig. 10.

As the Reynolds number slightly increases, the upper branches have numerous turning points. In the LES models, we assume that the grid scale lies within the inertial range of turbulence. At low Reynolds numbers, however, the sub-grid scale is comparable to the viscous scale, and the model assumption is not valid. In this sense, the failure of the eddy viscosity model is reasonable. We stopped tracking the upper branches, but continue to track the lower branch, i.e., the LES gentle UPO.

It is easy to track the branch of the gentle UPO without eddy viscosity because the lower-branch solution does not have small-scale structures. Since, as shown in the Introduction, the active UPO of the saddle-node pair with the gentle UPO describes the low Reynolds turbulence, we expect that the LES active UPO could represent the high Reynolds turbulence. Using the Smagorinsky constant as the bifurcation parameter at the moderately high Reynolds number, we find out the LES active UPO arising from the LES gentle UPO through the saddle-node bifurcation. The bifurcation structure of the LES gentle and active UPOs seems similar for different resolutions. These branches could be rescaled with the Smagorinsky mixing length $\langle\Delta\rangle C_S$. Here $\langle\Delta\rangle$ is the averaged filter width. This result suggests that if we use the sufficient number of grid points, the eddy viscosity does not violate bifurcation structure. Using the UPO analysis we could examine adequate resolutions in terms of the phase-space structure in the LES system.

At the large Smagorinsky constant, the eddy viscosity quenches the small-scale structure, so the flow structures of the LES active UPO seems similar to that of the NS active UPO at the low Reynolds number. When we decrease the Smagorinsky constant, however, we discover that the LES active UPO possesses the spanwise vortices which appear in the central region of the channel and seem to be caused by the streak instability [41]. The spanwise vortices are stretched by the streamwise vortices, leading to the high-Reynolds-stress objects attached to the walls. This result suggests that the spanwise vortices of the LES active UPO enhance the transfer of the streamwise turbulent momentum as in developed wall turbulence.

We should note that the mean and RMS velocities of the LES active UPO do not approximate those of the NS turbulence. As the Smagorinsky constant decreases we identify a lots of turning points because of the lack of resolution. We need to increase the number of grid points, but it is practically hard using our present computational resources. It may be a future research to develop more powerful numerical methods of the UPO analysis.

At the high Reynolds number, the LES active UPO describes the creation of the spanwise vortices which enhance turbulent momentum transfer. In fully developed turbulence, the spanwise vortices have been observed mainly in the overlap region apart from the wall [43]. We expect that the spanwise vortices of the LES active UPO could capture the key events of developed turbulence, although it is not clear whether the dynamics of the present UPO is strictly consistent with that in near-wall turbulence at higher Reynolds numbers. We need to further increase the Reynolds number, and moreover it is required to investigate UPOs for channel flow and turbulent boundary layer. The spanwise vortices in near-wall turbulence play important roles in the friction drag and heat transfer [44,45]. We believe that the dynamics of the spanwise vortices demonstrated by the present UPO gives some insights to improve the turbulent control strategies.

ACKNOWLEDGMENTS

This work was partially supported by JSPS KAKENHI Grant No. 50214672. The third author was supported by the European Research Council under the Coturb Grant No. ERC2014.AdG-669505.

[1] M. W. Hirsch, S. Smale, and R. L. Devaney, *Differential Equations, Dynamical Systems, and an Introduction to Chaos*, 3rd ed. (Academic Press, New York, 2012).

[2] S. Kato and M. Yamada, Unstable periodic solutions embedded in a shell model turbulence, Phys. Rev. E **68**, 025302(R) (2003).
[3] M. Kawasaki and S. I. Sasa, Statistics of unstable periodic orbits of a chaotic dynamical system with a large number of degrees of freedom, Phys. Rev. E **72**, 037202 (2005).
[4] J. Jiménez and P. Moin, The minimal flow unit in near-wall turbulence, J. Fluid Mech. **225**, 213 (1991).
[5] J. M. Hamilton, J. Kim, and F. Waleffe, Regeneration mechanisms of near-wall turbulence structures, J. Fluid Mech. **287**, 317 (1995).
[6] M. Nagata, Three-dimensional finite-amplitude solutions in plane Couette flow: bifurcation from infinity, J. Fluid Mech. **217**, 519 (1990).
[7] R. M. Clever and F. H. Busse, Tertiary and quaternary solutions for plane Couette flow, J. Fluid Mech. **344**, 137 (1997).
[8] F. Waleffe, Three-Dimensional Coherent States in Plane Shear Flows, Phys. Rev. Lett. **81**, 4140 (1998).
[9] G. Kawahara and S. Kida, Periodic motion embedded in plane Couette turbulence: Regeneration cycle and burst, J. Fluid Mech. **449**, 291 (2001).
[10] D. Viswanath, Recurrent motions within plane Couette turbulence, J. Fluid Mech. **580**, 339 (2007).
[11] G. Kawahara, M. Uhlmann, and L. van Veen, The significance of simple invariant solutions in turbulent flows, Annu. Rev. Fluid Mech. **44**, 203 (2012).
[12] O. Dauchot and F. Daviaud, Finite amplitude perturbation and spots growth mechanism in plane Couette flow, Phys. Fluids **7**, 335 (1995).
[13] Y. Duguet, P. Schlatter, and D. S. Henningson, Formation of turbulent patterns near the onset of transition in plane Couette flow, J. Fluid Mech. **650**, 119 (2010).
[14] E. Brand and J. F. Gibson, A doubly localized equilibrium solution of plane Couette flow, J. Fluid Mech. **750**, R3 (2014).
[15] M. Avila, F. Mellibovsky, N. Roland, and B. Hof, Streamwise-Localized Solutions at the Onset of Turbulence in Pipe Flow, Phys. Rev. Lett. **110**, 224502 (2013).
[16] S. Zammert and B. Eckhardt, Streamwise and doubly-localised periodic orbits in plane Poiseuille flow, J. Fluid Mech. **761**, 348 (2014).
[17] S. Okino, Kôkyûroku, RIMS, Kyoto University (in Japanese) 1994, 24 (2015), http://hdl.handle.net/2433/223841.
[18] J. Lustro, G. Kawahara, L. van Veen, M. Shimizu, and H. Kokubu, The onset of transient turbulence in minimal plane Couette flow, J. Fluid Mech. **862**, R2 (2019).
[19] B. Eckhardt and S. Zammert, Small scale exact coherent structures at large Reynolds numbers in plane Couette flow, Nonlinearity **31**, R66 (2018).
[20] G. Kawahara, Laminarization of minimal plane Couette flow: Going beyond the basin of attraction of turbulence, Phys. Fluids **17**, 041702 (2005).
[21] M. Linkmann, F. Knierim, S. Zammert, and B. Eckhardt, Linear feedback control of invariant solutions in channel flow, J. Fluid Mech. **900**, A10 (2020).
[22] J. Smagorinsky, General circulation experiments with the primitive equations: I. The basic experiment, Mon. Weather Rev. **91**, 99 (1963).
[23] D. K. Lilly, On the application of the eddy viscosity concept in the inertial sub-range of turbulence, Technical Report, NCAR manuscript 123, Boulder, CO (1966), doi: 10.5065/D67H1GGQ.
[24] J. W. Deardorff, A numerical study of three-dimensional turbulent channel flow at large Reynolds numbers, J. Fluid Mech. **41**, 453 (1970).
[25] C. Härtel and L. Kleiser, Analysis and modelling of subgrid-scale motions in near-wall turbulence, J. Fluid Mech. **356**, 327 (1998).
[26] M. Germano, U. Piomelli, P. Moin, and W. H. Cabot, A dynamic subgrid-scale eddy viscosity model, Phys. Fluid A **3**, 1760 (1991).
[27] S. Stolz, N. A. Adams, and L. Kleiser, An approximate deconvolution model for large-eddy simulation with application to incompressible wall-bounded flows, Phys. Fluids **13**, 997 (2001).
[28] H. Kobayashi, The subgrid-scale models based on coherent structures for rotating homogeneous turbulence and turbulent channel flow, Phys. Fluids **17**, 045104 (2005).

[29] Z. Wang, K. Luo, D. Li, J. Tan, and J. Fan, Investigations of data-driven closure for subgrid-scale stress in large-eddy simulation, Phys. Fluids **30**, 125101 (2018).
[30] X. I. A. Yang, S. Zafar, J.-X. Wang, and H. Xiao, Predictive large-eddy-simulation wall modeling via physics-informed neural networks, Phys. Rev. Fluids **4**, 034602 (2019).
[31] S. Rawat, C. Cossu, Y. Hwang, and F. Rincon, On the self-sustained nature of large-scale motions in turbulent Couette flow, J. Fluid Mech. **782**, 515 (2015).
[32] Y. Hwang, A. P. Willis, and C. Cossu, Invariant solutions of minimal large-scale structures in turbulent channel flow for Re_τ up to 1000, J. Fluid Mech. **802**, R1 (2016).
[33] L. van Veen, A. Vela-Martín, and G. Kawahara, Time-Periodic Inertial Range Dynamics, Phys. Rev. Lett. **123**, 134502 (2019).
[34] Q. Yang, A. P. Willis, and Y. Hwang, Exact coherent states of attached eddies in channel flow, J. Fluid Mech. **862**, 1029 (2019).
[35] P. Moin and J. Kim, Numerical investigation of turbulent channel flow, J. Fluid Mech. **118**, 341 (1982).
[36] E. R. van Driest, On turbulent flow near a wall, J. Aeronaut. Sci. **23**, 1007 (1956).
[37] E. Sasaki, G. Kawahara, A. Sekimoto, and J. Jiménez, Unstable periodic orbits in plane Couette flow with the smagorinsky model, J. Phys.: Conf. Ser. **708**, 012003 (2016).
[38] J. Gullbrand and F. K. Chow, The effect of numerical errors and turbulence models in large-eddy simulations of channel flow, with and without explicit filtering, J. Fluid Mech. **495**, 323 (2003).
[39] S. Toh and T. Itano, A periodic-like solution in channel flow, J. Fluid Mech. **481**, 67 (2003).
[40] V. Avsarkisov, S. Hoyas, M. Oberlack, and J. P. García-Galache, Turbulent plane Couette flow at moderately high Reynolds number, J. Fluid Mech. **751**, R1 (2014).
[41] G. Kawahara, J. Jiménez, M. Uhlmann, and A. Pinelli, Linear instability of a corrugated vortex sheet - a model for streak instability, J. Fluid Mech. **483**, 315 (2003).
[42] A. Lozano-Durán, O. Flores, and J. Jiménez, The three-dimensional structure of momentum transfer in turbulent channels, J. Fluid Mech. **694**, 100 (2012).
[43] Y. Wu and K. T. Christensen, Population trends of spanwise vortices in wall turbulence, J. Fluid Mech. **568**, 55 (2006).
[44] R. García-Mayoral and J. Jiménez, Drag reduction by riblets, Philos. Trans. R. Soc. A **369**, 1412 (2011).
[45] A. Yamamoto, Y. Hasegawa, and N. Kasagi, Optimal control of dissimilar heat and momentum transfer in a fully developed turbulent channel flow, J. Fluid Mech. **733**, 189 (2013).